Quantum Circuit Transformation Based on Subgraph Isomorphism and Tabu Search

Michael Shell, *Member, IEEE,* John Doe, *Fellow, OSA,* and Jane Doe, *Life Fellow, IEEE*

Abstract—The goal of quantum circuit transformation is to construct mappings from logical quantum circuits to physical ones in an acceptable amount of time, and in the meantime to introduce as few auxiliary gates as possible. We present an effective approach to constructing the mappings. It consists of two keys steps: one makes use of a combined subgraph isomorphism and complement (CSIC) to initialize a mapping, the other dynamically adjusts the mapping by using a Tabu search based adjustment (TSA). Our experiments show that, compared with the wghtgraph recently considered in the literature, CSIC can save 22.26% of auxiliary gates and reduce the depths of output circuits by 11.76% on average in the initialization of the mapping, and TSA has a better scalability than many state-of-the-art algorithms for adjusting mappings.

Index Terms—Quantum circuit transformation , Subgraph isomorphism , Initial mapping , Tabu search

I. INTRODUCTION

The entanglement of a quantum system with its surrounding environment will lead to quantum decoherence. It is unrealistic to use quantum error correction in circuit mapping process, since there are only dozens of available qubits for quantum devices in the NISQ era [1]. It is necessary to transform circuits by adding auxiliary gates to satisfy both logical and physical constraints, since quantum algorithms do not consider any hardware connectivity constraints. Hence, quantum circuit transformation is an important part of quantum circuit compilation. We need a set of highly efficient and automatic mapping procedures and adjustment routines to perform circuit transformation. In this process noise may be introduced, which brings a huge challenge to circuit compilation because noise has a significant impact on the final circuit and may make the result meaningless.

In the current work, we adjust the lifetime of qubits through parallelization, and use SubgraphMatching [2] to generate partial isomorphic subgraphs of logical circuits and physical circuits as part of the initial mapping. The advantage of the initial mapping result is that we use the appropriate subgraph isomorphism and the two-way connection of the logical circuit and the physical circuit to obtain a dense initial mapping, which avoids certain nodes from being mapped to remote locations. We use Tabu search [3] to generate circuits that can be executed on physical devices. Tabu search can avoid falling into local optimum and swapping the recently swapped qubits, thereby improve the parallelism of quantum gates. We add SWAP gates associated with the gates on the shortest path

to the candidate set, which greatly reduces the search space and improves the search speed. Our heuristic function not only considers the current gates but also the constraints of the gates already considered.

We compare CSIC with the state-of-the-art initial mapping methods wghtgraph [4] and optm [5]. On average, the auxiliary gates of the CSIC algorithm are reduced by 22.44% (resp. 27.02%), and the depths are reduced by 11.25% (resp. 14.12%). We compare TSA with wgtgraph [4] and SABRE [6]. On the one hand, TSA can handle 159 circuits in a few minutes, while the other two adjustment algorithms are difficult to handle medium-sized or large circuits. On the other hand, the number of SWAP gates added by wgtgraph is 26.87% (resp. 24.89%) smaller than that of TSA on average. Among the 159 circuits that we also test with SABRE, only 29 can be successfully mapped within the five-minute limit.

The main contributions of this paper are as follows.

1) We propose to use the combined subgraph isomorphism algorithm to generate part of the initial mapping and then complete the mapping based on the connectivity between qubits.
2) We present a heuristic circuit adjustment algorithm based on Tabu search [3], which can handle large circuits in a shorter time at a lower cost, compared with existing precise search and heuristic algorithms.
3) We put forward a look-ahead heuristic function that considers both the current gates and the gates yet to be processed. It filters out SWAP gates that are beneficial to the current gates and also bring closer the gates to be processed.
4) We test 159 circuits, and the results show that the initial mapping generated by our method requires to insert fewer SWAP gates, and the adjustment algorithm can be extended to handle medium-sized and large circuits.

The rest of this paper is organized as follows. In Section II we discuss some related work. In Section III we recall some background of quantum computing and quantum information. In Section IV we introduce the problem of quantum circuit transformation provide our solution by describing our algorithm in detail. The experimental results are reported in Section V. The last section concludes the paper and discusses some future research.

II. RELATED WORK

Quantum technology has been applied in practice, but large quantum computers have not yet been built. Most of the contributions of quantum information to computer science are still in the theoretical stage. In 2017, IBM developed the first

M. Shell was with the Department of Electrical and Computer Engineering, Georgia Institute of Technology, Atlanta, GA, 30332 USA e-mail: (see http://www.michaelshell.org/contact.html).
J. Doe and J. Doe are with Anonymous University.

5-qubit backend called IBM QX2, followed by the 16-qubit backend IBM QX3. The revised versions of them are called IBM QX4 and IBM QX5, respectively. IBM Q Experience [7] provides the public with free quantum computer resources on the cloud and opens source the quantum computing software framework Qiskit [8].

Users of these early quantum computers mainly rely on quantum circuits to implement quantum algorithms. They design logical circuits which then go through the step of circuit transformation in order to map logical qubits to physical ones before the logical circuits are executed in physical devices. A big challenge for quantum information is the problem of quantum decoherence. Due to the decoherence of qubits, quantum gates need to be applied in a coherent period as the time for a qubit to stay in a coherent state is very short. The longest coherence time of a superconducting quantum chip is still within 10us-100us.

There are several initial mapping methods. Paler [9] has showed that the initial mapping has an important influence on quantum circuit transformation. He proposed a heuristic method to find the initial mapping. Just by placing qubits in different positions from the default trivial placement in the actual circuit instances on the actual NISQ device, the time cost can be reduced by up to 10%. Li et al. [6] have proposed a novel reverse traversal technique, which determines the initial mapping by considering the entire circuit. Zhou et al. [10] have put forward an annealing algorithm to find an initial mapping, but it is unstable. In [4], Li et al. have considered the subgraph isomorphism algorithm wghtgraph to generate an initial mapping, which is the most recent result, so we will compare with it.

The goal of circuit adjustment algorithm is to minimize the number of auxiliary SWAP gates. There are currently five main methods for solving the quantum circuit adjustment problem.

- *Unitary matrix decomposition algorithm.* It is used in [11], [12] to rearrange the quantum circuit from the beginning while retaining the input circuit. It can be applied to a broad class of circuits consisting of generic gate sets, but the results are not as efficient as a compiler designed specifically for this task.
- *Converting into some existing problems.* This approach converts the quantum circuit transformation problem into some existing problems, such as AI planning [13], [14], Integer Linear Programming (ILP) [15], or Satisfiability Modulo Theories (SMT) [16]. Existing tools for those problems are then used to find acceptable results. The approach cannot take advantage of certain properties of quantum mapping, which is a drawback. Furthermore, as the time cost is usually long, it can only handle small quantum circuits.
- *Exact methods.* Siraichi et al. [17] have proposed an exact method. It will iterate all possible mappings for all dependencies, so it is only suitable for simple quantum architecture and cannot be extended to complex quantum architectures.
- *Graph theory.* In [18], Shafaei et al. have used the minimum linear permutation solution in graph theory to model the problem of reducing the interaction distance.

The idea is to first divide a given circuit into several subcircuits and apply the minimum linear permutation solution, respectively. Then we turn non-adjacent gates in the subcircuits into adjacent gates by adding auxiliary gates. Finally, we can use the minimum linear permutation solution to find an appropriate permutation and use bubble sort to calculate the number of necessary SWAP gates. In [19], [20], a two-step method is used to reduce the quantum circuit transformation to the graph problem to minimize the number of auxiliary gates, based on the graph coloring problem and the largest subgraph isomorphism problem.

- *Heuristic search.* Heuristic search uses an evaluation function to obtain an acceptable solution in exponential time. Zulehner et al. [5] have suggested to layer the circuits, then determine compatible mappings for each of these layers to add as few auxiliary gates as possible. Zhou et al. [10] have designed a heuristic search algorithm with a novel selection mechanism. Instead of choosing the operation with the lowest cost to apply, one can look forward one step and then choose the best continuous operation. In this way, the algorithm can effectively avoid local minimum. Moreover, a pruning mechanism is introduced to reduce the search space's size and ensure that the program terminates in a reasonable amount of time.

Li et al. [6] have proposed a SWAP-based search algorithm SABRE. Compared with previous search algorithms based on exhaustive mapping, SABRE can adapt to large quantum circuits in the NISQ era. In [21], a routing algorithm called $t\,|ket\rangle$ ensures that any quantum circuit can be compiled into any architecture. The algorithm is divided into four stages: decomposing the input circuit into time steps, determining the initial mapping, routing across time steps, and finally cleaning up. The heuristics in $t\,|ket\rangle$ give the same or better results than other circuit transformation systems in terms of the depth and the total number of gates in the compiled circuit, with much shorter running time, and can handle larger circuits. In [22], a variation-aware qubit movement strategy is proposed. It takes advantage of the change in error rate and a change-aware quantum circuit transformation strategy by trying to select the route with the lowest probability of failure. This strategy uses the error rate of SWAPs to allocate logical qubits to physical qubits, thus avoiding paths with high error rates as much as possible.

Among the existing methods above, wghtgraph [4] and optm [5] are probably the most effective initial mapping ones. As to circuit adjustment algorithms, wgtgraph [4] and SABRE [6] represent the state of the art. Therefore, we choose to compare our solution with them in Section V.

III. PRELIMINARY

In this section we introduce some notions and notations of quantum computing and quantum information. Classical information is stored in bits, while quantum information is stored in qubits. Besides two basic states $|0\rangle$ and $|1\rangle$, a qubit
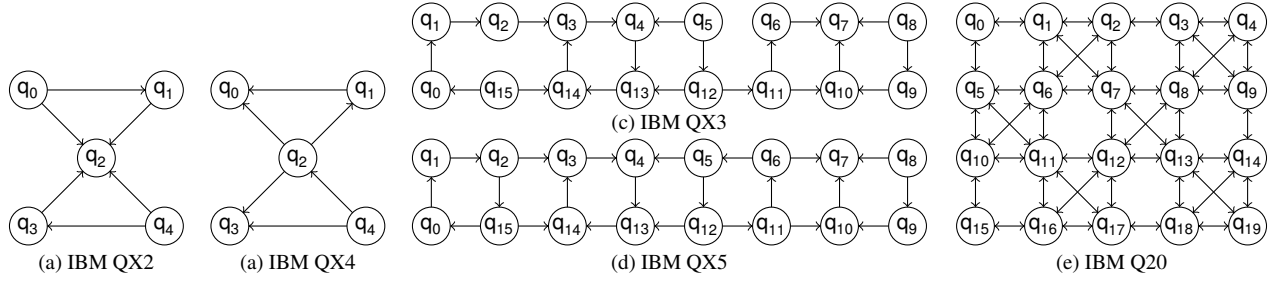
Fig. 1: IBM QX architectures

(a) IBM QX2 (a) IBM QX4 (c) IBM QX3 (d) IBM QX5 (e) IBM Q20

can be in any linear superposition state like $|\phi\rangle = a\,|0\rangle + b\,|1\rangle$, where $a, b \in \mathbb{C}$ satisfy the condition $|a|^2 + |b|^2 = 1$. The intuition is that $|\phi\rangle$ is in the state $|0\rangle$ with the probability $|a|^2$ or in the state $|1\rangle$ with the probability $|b|^2$. We use letters q and q in different fonts to represent physical qubits and logical qubits.

By applying quantum gates to qubits, we can change their states. For example, the Hadamard gate (H gate) can be applied on a single qubit, while the CNOT gate can be applied on two qubits. Their representations in terms of gate symbols and their semantics in terms of matrices are shown in Fig. 2.
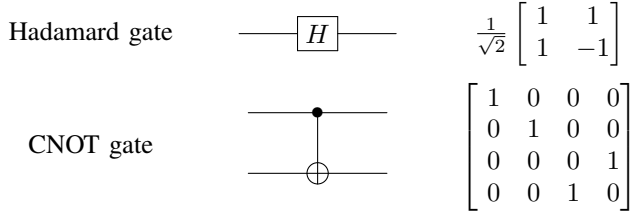

Fig. 2: The symbols of two quantum gates and their matrices

A quantum logical circuit consists of quantum gates inter-connected by quantum wires [23]; see Fig. 3 for an example. A quantum wire is a mechanism for moving quantum data from one location to another. Each line represents a qubit, and the gates on the lines act on the corresponding qubits. The execution order of a quantum logical circuit is from left to right. The width of a circuit refers to the number of qubits in the circuit. The depth of a circuit refers to the number of layers executing in parallel. For example, the depth of the circuit in Fig. 3 is 6, and the width is 5. In this paper, a circuit with a depth less than 100 is a called a small circuit, a circuit with a depth greater than 1000 is called a large circuit, and the rest are medium-sized circuits. It is unnecessary to consider quantum gates acting on single qubits in circuit adjustments, since the single qubits are local [18].

In the current work, we mainly consider the physical circuits of the IBM Q series. Let $\mathcal{AG}_{\mathcal{P}} = (V_P, E_P)$ denote the architecture graph of a physical circuit, where V_P denotes the set of physical qubits and E_P denotes the set of edges that connect CNOT gates. In Fig. 1, diagrams (a) and (b) are the physical architecture graphs of the 5-qubit IBM QX2 and IBM QX4, respectively; diagrams (c) and (d) are the physical architecture graphs of the 16-qubit IBM QX3 and IBM QX5, respectively; diagram (e) is the physical architecture graph of
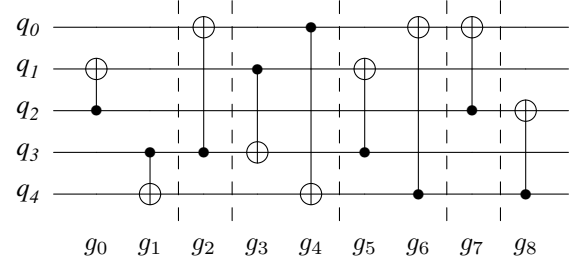
Fig. 3: A quantum circuit

IBM Q20. The direction in each edge indicates the control direction of a 2-qubit gate, and 2-qubit gates can only be performed between qubits with edges connected. IBM physical circuits only support single quantum gates and CNOT gates between two adjacent qubits.
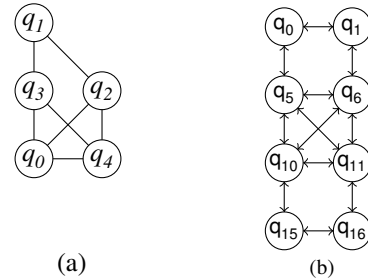
Fig. 4: (a) The architecture graph of original circuit in Fig. 3. (b) The partial architecture graph of IBM Q20.

Given a logical circuit LC, a physical structure $\mathcal{AG}_P$, an initial mapping τ, and a CNOT gate $g = \langle q_i, q_j \rangle$, where q_i is the control qubit, q_j is the target qubit, if gate g is executable on a physical circuit with the structure $\mathcal{AG}_P$, then $\langle \tau(q_i), \tau(q_j) \rangle$ must be a directed edge on $\mathcal{AG}_P$.

Example 3.1: Fig. 4 (a) is the logical structure of Fig. 3. Fig. 4 (b) is the partial architecture graph of IBM Q20. An initial mapping is

$$\tau = \{q_0 \rightarrow \mathsf{q}_{10},\ q_1 \rightarrow \mathsf{q}_0,\ q_2 \rightarrow \mathsf{q}_6,\ q_3 \rightarrow \mathsf{q}_5,\ q_4 \rightarrow \mathsf{q}_{11}\}.$$

The 2-qubit gate $g_0 = \langle q_2, q_1 \rangle$ is not executable, since the edge $\langle \tau(q_2), \tau(q_1) \rangle = \langle \mathsf{q}_6, \mathsf{q}_0 \rangle$ does not exist in $\mathcal{AG}_P$. But $g_3 = \langle q_1, q_3 \rangle$ is executable, since the edge $\langle \tau(q_1), \tau(q_3) \rangle = \langle \mathsf{q}_0, \mathsf{q}_5 \rangle$ exists in $\mathcal{AG}_P$.

IV. QUANTUM CIRCUIT TRANSFORMATION

A common assumption for circuit transformation is that we are given a circuit that has only single quantum gates and CNOT gates [24], [25]. We add auxiliary gates to move two non-adjacent qubits to adjacent positions or change the direction of a CNOT gate. Adding more gates increases the risk of introducing more noise. Therefore, we hope to find a circuit transformation algorithm that, when given an input circuit, can produce an output circuit with a minimal number of auxiliary gates and a small circuit depth in an acceptable amount of time.

Roughly speaking, quantum circuit transformation includes the following three steps.

1) *Preprocessing.* This step includes extracting the logical architecture graph of the circuit, adjusting the life cycle of qubits as in [26], and calculating the shortest paths of the physical circuit.

2) *Isomorphism and completion.* This step uses the subgraph isomorphism algorithm to find part of the initial mapping [2]. Then we perform a mapping completion to include the remaining nodes that do not satisfy all isomorphism requirements, according to the connectivity between the unmapped node and the mapped nodes.

3) *Adjustment.* After the second step, some logically adjacent nodes may be mapped to physically non-adjacent nodes, thus quantum gates applied on them cannot be executable on physical devices. It is necessary to adjust the quantum circuits by adding auxiliary gates to swap qubits. We use Tabu search for the adjustment so as to generate circuits that can be physically executed.

Note that isomorphism and adjustment are both NP-complete [17]. So we make use of some heuristics. Below we give a detailed account of each of the steps.

A. Preprocessing

In the preprocessing step, we adjust the input circuit described by an openQASM program to shorten the life cycle of qubits. Then we use a Breadth-First Search (BFS) to calculate the shortest distance between each pair of nodes on the architecture graph.

We use a layered method to analyze the life cycle of qubits and pack the gates that can be executed in parallel into a $bundle$, forming a layered bundle format [26]. A conversion method is designed to use the layered bundle format to determine which gates can be moved so the qubits related to these gates can reduce their life cycles, and the execution time of quantum programs can also be reduced.

Quantum gates acting on different qubits can be executed in parallel. Therefore, we classify the gates that can be executed in parallel into one layer, otherwise we add a new layer. The notation $L(LC) = \{\mathcal{L}_0, \mathcal{L}_1, ..., \mathcal{L}_n\}$ represents the layered circuit, where $\mathcal{L}_i$ $(0 \leq i \leq n)$ stands for a quantum gate set that can be executed in parallel. The quantum gate set separated by the dotted line in Fig. 3 are the following $\mathcal{L}_0 = \{g_0, g_1\}, \mathcal{L}_1 = \{g_2\}, \mathcal{L}_2 = \{g_3, g_4\}, \mathcal{L}_3 = \{g_5, g_6\}, \mathcal{L}_4 = \{g_7\}, \mathcal{L}_5 = \{g_8\}$.

At the same time of circuit layering, we generate a logical circuit architecture graph $\mathcal{AG}_\mathcal{L} = (V_L, E_L)$, which is an undirected graph with V_L being the set of vertices, and E_L the set of undirected edges that represent the connectivity between qubits related by CNOT gates. Given a physical architecture graph and assume the distance of each edge is 1, we can use Floyd-Warshall algorithm to calculate the shortest distance matrix $dist[i][j]$, which represents the shortest distance from q_i to q_j.
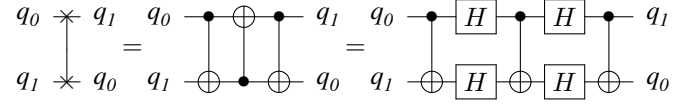

Fig. 5: Implenting a SWAP gate by using CNOT gates and H gates

For IBM QX2, QX3, QX4, and QX5, the control of one qubit to a neighbour is unilateral. In this case, a SWAP gate can be implemented by using three CNOT gates and four H gates, as shown in Fig. 5. The four H gates are needed to change the direction of the middle CNOT gate. Consider a CNOT gate $g = \langle q_i, q_j \rangle$. If q_i and q_j are mapped to q_m and q_n, respectively, then the cost of executing g under the shortest path is $cost_{cnot}(q_i, q_j) = 7 \times (dist[m][n] - 1)$. For IBM Q20, where the control between two adjacent qubits are bilateral, a SWAP gate can be implemented by using three CNOT gates. Thus the cost is $cost_{cnot}(q_i, q_j) = 3 \times (dist[m][n] - 1)$.

Example 4.1: Take the QX5 (cf. Fig. 1 (d)) structure as an example. Suppose there is a CNOT gate $g = \langle q_1, q_2 \rangle$, with q_1 mapped to q_1 and q_2 mapped to q_{14}. The shortest distance between them is $dist[1][14] = 3$. There are 3 shortest paths to move q_1 to an adjacent position of q_{14}: $\pi_0 = q_1 \rightarrow q_2 \rightarrow q_3 \rightarrow q_{14}$, $\pi_1 = q_1 \rightarrow q_2 \rightarrow q_{15} \rightarrow q_{14}$, $\pi_2 = q_1 \rightarrow q_0 \rightarrow q_{15} \rightarrow q_{14}$. Their costs are given by $cost_{\pi_0} = 18$, $cost_{\pi_1} = 14$, and $cost_{\pi_2} = 14$, respectively.

B. Isomorphism and Completion

In general, in a physical architecture graph, it is almost impossible to find a subgraph that exactly matches all the nodes in a logical architecture graph. We regard the mapping with the largest number of matching nodes as the partial mapping. SubgraphMatching compares various compositions of several state-of-the-art subgraph isomorphism algorithms. It shows that the best performance can be achieved by using filters and the sorting ideas of the GraphQL algorithm to process candidate nodes, and the local candidates calculation method LFTJ based on set-intersection to enumerate the results. Since SubgraphMatching cannot handle disconnected graphs, we artificially create connected graphs by connecting isolated nodes to the nodes with the largest degree in the logical architecture graph.

The input of Algorithm 29 is a target graph ($\mathcal{AG}_P$), a query graph ($\mathcal{AG}_L$), and the partial mapping set T. First, we initialize an empty queue Q. Then we traverse τ and add the unmapped nodes to the queue Q. For the unmapped nodes, we try to map them to the vicinity of the mapped nodes in $\mathcal{AG}_P$. If a node q is not mapped to any physical node, we need to perform such kind of mapping completion. Finally, we generate a

---

Algorithm 1: Complete initial mapping

Input: $\mathcal{AG}_{\mathcal{L}}$: The architecture of logical circuit
$\mathcal{AG}_{\mathcal{P}}$: The architecture of physical circuit
T: A partial mapping set obtained by
SubgraphMatching

Output: $result$: A collection of mapping relations
between $\mathcal{AG}_{\mathcal{L}}$ and $\mathcal{AG}_{\mathcal{P}}$

1 **Initialize** $result = \emptyset$;
2 $l \leftarrow \max_{\tau \in T} \ \tau.length$;
3 **for** $\tau \in T$ **do**
4   **if** $l = \tau.length$ **then**
5        $result.add(\tau)$;
6        $Q \leftarrow$ an empty unmapped node queue
7        $i \leftarrow 1$;
8   **while** $i \leq \tau.length$ **do**
9           $Q.push(\{i, \ i \leq \tau.length \ \})$
10           $i \leftarrow i + 1$;
11   **while** Q *is not empty* **do**
12           $q \leftarrow Q.poll()$;
13           $targetAdj \leftarrow \mathcal{AG}_{\mathcal{P}}.adjacencyMatrix()$;
14           $queryAdj \leftarrow \mathcal{AG}_{\mathcal{L}}.adjacencyMatrix()$;
15           $cans \leftarrow$ an empty candidate node list
            sorted by degree
16           $cans \cup \{q_m, \ q_m \leq queryAdj[q].length\}$;
17   **while** $cans$ *is not empty* **do**
18              $q \leftarrow \tau[cans.first]$;
19              $k \leftarrow 0$;
20              $cans \leftarrow cans \backslash cans.first$;
21   **while** $k < targetAdj[q].length$ **do**
22   **if** $(targetAdj[q][k] \neq$
                   -1 *or* $targetAdj[k][q] \neq -1)$
23   *and not* $\tau.contains(k)$ **then**
24                    $\tau[q] \leftarrow k$;
25   break;
26                 $k \leftarrow k + 1$;
27   **if** $k \neq targetAdj[q].length$ **then**
28   break;

29 **return** $result$;

---

dense mapping, which can reduce the added auxiliary gates. In principle, we could try to match the remaining unmapped nodes randomly, but it may lead to a mapping with a node far away from other nodes. If an unmapped node has an edge adjacent to a matched node in the query graph, it will be matched to one of the adjacent nodes first. In this way, we can obtain all initial candidate mappings.

Example 4.2: Following the previous example, we first use the CSIC algorithm for the logical architecture graph given in Fig. 4 (a) and the physical architecture graph given in Fig. 1 (e) to obtain the partial mapping set $T = \{\tau_0, \tau_1, ..., \tau_n\}$. We take one of the partial mappings as an example.

$$\tau_0 = \{q_0 \rightarrow \mathsf{q}_{10}, q_1 \rightarrow -1, q_2 \rightarrow \mathsf{q}_6, q_3 \rightarrow \mathsf{q}_5, q_4 \rightarrow \mathsf{q}_{11}\}.$$

Here $q_1 \rightarrow -1$ means that q_1 is not mapped to any physical

node, so we need to perform a mapping completion. In this example, the maximum number of mapped nodes is 4. Next, we demonstrate how τ_0 is completed. We add all unmapped nodes to the queue Q. In this example, $Q = \{q_1\}$. Then we loop until Q is empty. We pop the first element q of Q, get the adjacency matrix of the query graph and the target graph, and traverse the adjacency matrix. We put the nodes q_m adjacent to q into the candidate nodes list $cans$, which is sorted by the connectivity of q_m and q. We get $cans = \{q_3, q_2, q_4, q_0\}$. Thereafter, we traverse $cans$ and take out of the first element q_3 in $cans$, and calculate the phycial node $\mathsf{q} = \mathsf{q}_5$, $\tau_0(q_3) = \mathsf{q}_5$. Finally, we map q to the node connected to q but not yet mapped. If the nodes connected to q have been mapped, the loop continues. In this example, it can be directly mapped to q_0. In the end, we obtain the mapping $\tau_0 = \{q_0 \rightarrow \mathsf{q}_{10}, q_1 \rightarrow \mathsf{q}_0, q_2 \rightarrow \mathsf{q}_6, q_3 \rightarrow \mathsf{q}_5, q_4 \rightarrow \mathsf{q}_{11}\}$.

C. Adjustment

1) Tabu search: The Tabu search algorithm is a type of heuristic algorithm. It uses a tabu list to avoid searching repeated spaces, thereby avoiding deadlock. The algorithm uses amnesty rules to jump out of the local optimum to ensure the diversity of transformed results. The circuit adjustment mainly relies on the Tabu search algorithm, aiming to handle those large circuits that the current algorithm is difficult to handle and produce an output circuit closer to the optimum solution.

The following objects are defined in Tabu search: neighborhoods, neighborhood action, tabu list, candidate set, tabu object, evaluation function, and amnesty rule. All the edges that can be swapped in the current map are the neighborhoods. The tabu list avoids local optimum and guarantees the parallelism of auxiliary gates. The tabu object is the object in the tabu list. We try not to use the recently swapped qubits as much as possible, which are added to the tabu list. We perform pruning to reduce search space, because only swaps adjacent to at least one gate node are meaningful. We select the edge in the shortest path that has an intersection with the qubits contained in the gate as the candidate set. The evaluation function selects a SWAP evaluation formula from the candidate set, taking the objective function as the evaluation function in general. The evaluation function should meet the requirements of some gates, and the number of SWAP gates added or the depth of the entire circuit should be small. The amnesty rules are used when all objects in the candidate set are banned, or after banning an object, the target value will be greatly reduced.

The calculation of the neighborhoods is shown in Algorithm 32. The input is the current circuit mapping τ_p. The variable $qubits$ contains the mapping of physical qubits to logical qubits, where $j = qubits[i]$ means that the i-th physical qubit has been mapped to the j-th logical qubit. The variable $locs$ represents the mapping of logical qubits to physical qubits, where $j = locs[i]$ means that the i-th logical qubit has been mapped to the j-th physical qubit. The current layer list of all gates is cl, and the output is a candidate set of the current mapping. The set E contains the edges of all the shortest paths in the physical architecture graph of all the gates in the current

---

Algorithm 2: Calculate the candidate sets

Input: $dist$: The shortest paths of physical architecture

$qubits$: The mapping from physical qubits to logical qubits

$locs$: The mapping from logical qubits to physical qubits

cl: Gates included in the current layer of circuits

Output: $results$: The set of candidate solution

1 **Initialize** $results \leftarrow \emptyset$;

2 $E_w \leftarrow$ Calculate the weight of each edge

3 $swap\_nodes \leftarrow$ An empty set of candidate swap nodes

4 **foreach** $g \in cl$ **do**

5   **if** g is executable **then**

6         $cl \leftarrow cl \backslash \{g\}$;

7   **else**

8         $q_1 \leftarrow locs[g.control]$;

9         $q_2 \leftarrow locs[g.target]$;

10         $swap\_nodes.add(q_1)$;

11         $swap\_nodes.add(q_2)$;

12 **foreach** $g \in cl$ **do**

13     $q_1 \leftarrow locs[g.control]$;

14     $q_2 \leftarrow locs[g.target]$;

15   **foreach** $path \in paths[q_1][q_2]$ **do**

16   **foreach** $e \in path$ **do**

17   **if** $\{sour\_node, tar\_node\} \cap swap\_nodes \neq \varnothing$ **then**

18                 $new\_qubits \leftarrow qubits$;

19                 $new\_locs \leftarrow locs$;

20                 $q_1 \leftarrow new\_qubits[e.source]$;

21                 $q_2 \leftarrow new\_qubits[e.target]$;

22                 $new\_qubits[e.source] \leftarrow q_2$;

23                 $new\_qubits[e.target] \leftarrow q_1$;

24   **if** $q_1 \neq -1$ **then**

25                     $new\_locs[q_1] \leftarrow q_2$;

26   **if** $q_2 \neq -1$ **then**

27                     $new\_locs[q_2] \leftarrow q_1$;

28                 $s \leftarrow \emptyset$;

29                 $s.swaps \leftarrow p.swaps \cup \{distance.paths[path_{index}][j]\}$;

30                 $s.value \leftarrow evaluate(dist, new\_locs, cl)$;

31                 $results \leftarrow results \cup \{s\}$;

32 **return** $results$;

---

layer. Lines 17-31 swap all the edges of candidate set, and calculate the cost of them.

Example 4.3: Let us consider the mapping

$$\tau_0 = \{q_0 \to \mathsf{q}_{10}, q_1 \to \mathsf{q}_0, q_2 \to \mathsf{q}_6, q_3 \to \mathsf{q}_5, q_4 \to \mathsf{q}_{11}\},$$

for $L_0 = \{g_0, g_1\}$, $dist_{cnot}(g_0) = 3$ and $dist_{cnot}(g_1) = 3$. Gate g_1 can be executed directly in the τ_0 mapping, so we delete it from L_0, but g_0 cannot be executed in the mapping τ_0. Thus, a circuit adjustment is required. Nodes that cannot be executed join the set $swap\_nodes = \{\mathsf{q}_0, \mathsf{q}_6\}$. The set of shortest paths is $paths = \{\{\mathsf{q}_6 \to \mathsf{q}_1 \to \mathsf{q}_0\}, \{\mathsf{q}_6 \to \mathsf{q}_5 \to \mathsf{q}_0\}\}$, and then we traverse the shortest paths to calculate the candidate set. The two endpoints of an edge passed by one of the shortest paths should intersect with the swap set and join the candidate set. The current candidate set is $\{(\mathsf{q}_6, \mathsf{q}_1), (\mathsf{q}_1, \mathsf{q}_0), (\mathsf{q}_6, \mathsf{q}_5), (\mathsf{q}_5, \mathsf{q}_0)\}$.

Algorithm 3: Tabu search

Input: τ_{ini}: The initial mapping

tl: Tabu list

Output: τ_{best}: The best mapping

1 **Initialize** $\tau_{best} \leftarrow \tau_{ini}$;

2 $iter \leftarrow 1$;   // Number of iterations

3 **while** not $mustStop(iter, \tau_{best})$ **do**

4     $C \leftarrow \tau_{ini}.candidates()$; // candidate set

5   **if** C is empty **then**

6         $break$;

7     $C_{best} \leftarrow find\_best\_candidates(C, tl)$;

8   **if** C_{best} is empty **then**

9         $C_{best} \leftarrow find\_amnesty\_candidates(C, tl)$;

10     $\tau_{best} \leftarrow C_{best}$;

11     $tl \leftarrow tl \cup \{C_{best}.swap\}$;

12     $iter \leftarrow iter + 1$;

13 **return** τ_{best}

The circuit mapping algorithm based on Tabu search takes a layered circuit and an initial mapping as input and outputs a circuit that can be executed in the specified architecture graph, as shown in Algorithm 13. The transformed circuit mapping of each layer is used as the initial mapping of the next layer. Line 1 regards the initial mapping τ_{ini} as the best mapping τ_{best}. Lines 3-12 cyclically check whether all all gates in the current layer can be executed under the mapping τ_{ini}. If not all the gates are executable or the number of iterations has not reached the given maximum number, the search will continue. Otherwise, the search will terminate. Line 4 gets the current mapping candidate, and Line 7 finds the best mapping in the candidate set. The mapping will first remove the overlapping elements of the candidate set and the tabu list. Then from the remaining candidates, we choose a mapping with the lowest cost. Line 9 are the amnesty rules. When the best candidate is not found, the candidate set elements are all the same as the tabu list elements. The amnesty rules select the mapping with the lowest cost in the candidate set as the best candidate mapping. Lines 10-12 update the best mapping τ_{best} and the current mapping τ_{curr}, and add the SWAP performed by the

best mapping to the tabu list tl, indicating that the SWAP has just been performed. The algorithm would try to avoid re-swapping the just swapped qubits. Then it will check whether the termination condition of the algorithm is satisfied. The condition determines whether the number of iterations has reached the maximum number, or the current mapping ensures all gates in the current layer can be executed.

Example 4.4: Let us continue the previous example. We start searching from the initial mapping. We need to get the candidate SWAP set and select the one with the lower evaluation scores. For $L_0 = \{g_0, g_1\}$, the candidate set is $\{(\mathsf{q_6}, \mathsf{q_1}), (\mathsf{q_1}, \mathsf{q_0}), (\mathsf{q_6}, \mathsf{q_5}), (\mathsf{q_5}, \mathsf{q_0})\}$, and the costs are given as follows.

$$cost((\mathsf{q_6}, \mathsf{q_1})) = 3.0, \ cost((\mathsf{q_1}, \mathsf{q_0})) = 3.0,$$
$$cost((\mathsf{q_6}, \mathsf{q_5})) = 3.0, \ cost((\mathsf{q_5}, \mathsf{q_0})) = 3.0.$$

The algorithm will choose the first SWAP, the mapping becomes

$$\tau_0 = \{q_0 \rightarrow \mathsf{q_{10}}, q_1 \rightarrow \mathsf{q_0}, q_2 \rightarrow \mathsf{q_1}, q_3 \rightarrow \mathsf{q_5}, q_4 \rightarrow \mathsf{q_{11}}\}.$$

It can be seen that the current mapping ensures the executability of g_0. The algorithm continues to search for the next layer.

2) Evaluation functions : We can control the search direction by changing the evaluation functions. We test two evaluation functions: one uses the number of auxiliary gates in the generated circuit as the evaluation criterion (1), and the other uses the depth of the generated circuit as the evaluation criterion (2).

$$cost((\mathsf{q_m}, \mathsf{q_n})) = \sum_{g \in L} (dist[\tau(g.control)][\tau(g.target)]) \quad (1)$$

$$cost((\mathsf{q_m}, \mathsf{q_n})) = Depth(L) \quad (2)$$

Here $cost((\mathsf{q_m}, \mathsf{q_n}))$ represents the cost of executing all the gates of the current layer L after swapping $\mathsf{q_m}$ with $\mathsf{q_n}$. We only calculate the depth between the unmapped gates as in (1) or the distance of the unmapped gates as in (2).

3) Look ahead : We observe that the number of gates in each layer after layering is small. The output of the i-th ($i < n$) layer is used as the input of the $(i+1)$-th layer. Note that any swap operation in the i-th layer will affect the mapping of the $(i+1)$-th layer. If we only consider the gates in the current layer when choosing the swapping gates, the swap only satisfies the requirement of the i-th layer, not necessarily the next layer. Therefore, we take the gates in the $(i+x)$-th ($i+x < n$) layer into consideration, where x is the number of forward-looking layers. However, it is necessary to give a higher priority to the execution of the gates in the i-th layer, so we introduce an attenuation factor δ, which controls the influence of the gates in the $(i+x)$-th layer. Heuristics show that for $x = 2$, $\delta = 0.9$, the final effect is approximately the best. Our evaluation functions in (1) and (2) can be adjusted as (3) and (4), respectively.

$$cost((\mathsf{q_m}, \mathsf{q_n})) = \sum_{g \in L_i} (dist[\tau(g.control)][\tau(g.target)]) +$$
$$\delta \times \sum_{j=i}^{i+x} \sum_{g \in L_j} (dist[\tau(g.control)][\tau(g.target)])$$
$$(3)$$

$$cost((\mathsf{q_m}, \mathsf{q_n})) = Depth(L_i) + \delta \times Depth(\sum_{j=i}^{i+x} L_j). \quad (4)$$

4) Complexity: Given a logical circuit architecture graph $\mathcal{AG_L} = (V_L, E_L)$ and a physical circuit architecture graph $\mathcal{AG_P} = (V_P, E_P)$, we assume that the initial mapping is τ, the depth of the circuit is d, and the number of qubits is V_L. Tabu search deals with one layer at a time, and searches at most d times. Starting from the initial mapping, we first delete the executable gates of the first layer under the initial mapping. Then, the edges of all the shortest paths of all the gates that are not executable in the current layer are added to the candidate set where at least one node is in the gate mapping. In the worst case, the length of the shortest path is $(|E_P|-1)$ and the size of the candidate set is $(|E_P|-1)$. Each SWAP will make the total distance between the gates smaller. In the worst case, the number of SWAPs is $(|E_P|-1)^{|E_P|-2}$, but our selection strategy will make the number of SWAPs significantly reduced. The time complexity in the worst case is $d \times (|E_P|-1)^{(|E_P|-2)}$, and the space complexity is the size of our candidate set $(E_P - 1)$.

V. EXPERIMENTS

We compare the CSIC algorithm and the circuit adjustment algorithm based on Tabu search TSA with the wghtgraph in [4] and the heuristic algorithm A^* in [5]. All the experiments are conducted on a Windows machine with 3.3GHz CPU and 10G memory.

First, we compare the efficiency of initial mapping on optm [5], CSIC and wghtgraph [4]. In order to observe the results of these two initial mapping algorithms, we used the same circuit adjustment algorithm A^* [5]. We have tested 159 circuits. Within five minutes, optm, wghtgraph, and CSIC can handle 121, 106, and 131 circuits, respectively. There are 103 circuits that they can handle. We then compare the wghtgraph algorithm and the CSIC algorithm more closely. The wghtgraph algorithm has 21 circuits with fewer auxiliary gates and 19 circuits with smaller depths, and the CSIC algorithm has 54 circuits with fewer auxiliary gates and 60 circuits with smaller depths. They output 25 circuits with equal depth and 29 circuits with equal auxiliary gates. On average, the auxiliary gates of the CSIC algorithm are reduced by 22.44%, and the depths are reduced by 11.25%. Next, we compare the optm algorithm with the CSIC algorithm. The optm algorithm has one circuit with fewer auxiliary gates and two circuits with a small depth, while the CSIC algorithm has 99 circuits with fewer auxiliary gates and 98 circuits with a small depth. They have 4 circuits with equal depth and 4 circuits with equal auxiliary gates. The auxiliary gates of the CSIC algorithm are relatively reduced by 27.02%, and the depths are reduced by 14.12%. Table I shows the experimental data on 104 circuits. The three initial mapping algorithms are compared according to the depths of the generated circuits using the same A^* algorithm, and the numbers of added auxiliary gates. The column headed by CSIC /optm shows the efficiency improvement of the former upon the latter $(n_{optm} - n_{CSIC})/n_{optm}$.

	optm	wgtgraph	CSIC	CSIC /optm	CSIC /wgtgraph
Depths	168895	163422	145040	14.12%	11.25%
Auxiliary gates	20439	19232	14916	27.02%	22.44%

TABLE I: Comparison of optm, wgtgraph and CSIC

benchmarks	#circ.	TSA_{num}		TSA_{dep}		wgtgraph		SABRE	
		#succ.	time	#succ.	time	#succ.	time	#succ.	time
small	66	66	32	66	29	64	587	23	12996
medium	49	49	45	49	40	35	1183	6	13019
large	44	44	407	44	432	0	-	0	1340719
total	159	159	484	159	501	99	-	29	1366734

TABLE II: Comparison of TSA_{num}, TSA_{dep}, wghtgraph and SABRE

We then compare in Table II the use of two indicators TSA_{dep} and TSA_{num} that prioritize smaller depths and fewer auxiliary gates, respectively. Using the two indicators as objective functions, we tested 159 circuits. The depths of the final circuits obtained by TSA_{num} are 1.93% smaller than TSA_{dep} on average, and the numbers of auxiliary gates added are 4.53% smaller on average. When inserting a SWAP gate, the circuit needs to add 3 CNOT gates, and the depth will be increased by 3. Therefore, if fewer SWAP gates are added, the depths of the circuits will reduce accordingly.

Finally, we compare TSA with wgtgraph. Since the wgtgraph algorithm only uses 2-qubit gates, it is impossible to compare the depths of the generated circuits. Instead, we compare the number of SWAP gates added and the time costs. We set a five-minute timeout period and tested 159 circuits. It turns out that TSA_{num} only takes 461 seconds and TSA_{dep} takes 485 seconds. The wgtgraph algorithm takes 1908 seconds for the 159 circuts, but only produces valid results for 99 circuits, including 64 small circuits, 35 medium-sized circuits, and no circuit output is produced for any of the 44 large circuits. Although Tabu search can quickly produce results on large circuits, in contrast, more auxiliary gates are added. In the generated circuits obtained by wgtgraph from 99 small and medium-sized circuits, the number of SWAP gates added by wgtgraph is 26.87% (resp. 24.89%) smaller than TSA_{num} (resp. TSA_{dep}) on average. The Tabu search can quickly output converted circuits on large circuits, but wgtgraph cannot get results in the predefined time bound. Since our candidate set is too small to be able to process the circuit quickly, but this also leads to an increase in the insertion of additional gates. As to SABRE, when dealing with 159 circuits with a five-minute limit for each circuit, it successfully produces results for only 23 small circuits, 6 medium-sized circuits, and 1 large circuit. The detailed results of the circuit comparisons are in the Appendices.

VI. CONCLUSION

We propose a scalable algorithm for quantum circuit transformation. First, we use a subgraph isomorphism algorithm and a mapping completion method based on the connectivity between qubits to generate a high-quality initial mapping. Secondly we exploit a look-ahead heuristic search taking into account the influence of the pre-layer circuit mapping to reduce the number of auxiliary gates, and complete the

transformation. Finally, we compare the influence of initial mapping with the state-of-the-art algorithm wghtgraph and optm and also compare the overall efficiency with optm, wghtgraph, and SABRE. Experimental results show that the initial mapping generated by CSIC have fewer SWAP gates inserted and the results can be obtained in an acceptable amount of time. Most small and medium-sized circuits can be handled in a few seconds. For large circuits, the results can be obtained within a few minutes, but the cost of insertion may be lareger than that of wgtgraph. We introduce a look-ahead method to make each selected SWAP more in line with the constraints of the gates to be processed. In the future, we will investigate how to reduce the number of inserted auxiliary gates and increase the speed. We will also apply the proposed method to more NISQ devices.

REFERENCES

[1] J. Preskill, "Quantum Computing in the NISQ era and beyond," *Quantum*, vol. 2, p. 79, 2018.
[2] S. Sun and Q. Luo, "In-memory subgraph matching: An in-depth study," in *Proceedings of the 2020 International Conference on Management of Data*. ACM, 2020, pp. 1083–1098.
[3] F. W. Glover, "Tabu search - part II," *Informs Journal on Computing*, vol. 2, no. 1, pp. 4–32, 1990.
[4] S. Li, Z. Xiangzhen, and Y. Feng, "Qubit mapping based on subgraph isomorphism and filtered depth-limited search," *IEEE Transactions on Computers*, pp. 1–1, 2020.
[5] A. Zulehner, A. Paler, and R. Wille, "An efficient methodology for mapping quantum circuits to the IBM QX architectures," *IEEE Transactions on Computer-Aided Design of Integrated Circuits and Systems*, no. 7, pp. 1226–1236, 2019.
[6] G. Li, Y. Ding, and Y. Xie, "Tackling the qubit mapping problem for nisq-era quantum devices," in *Proceedings of the 24th International Conference on Architectural Support for Programming Languages and Operating Systems*. ACM, 2019, pp. 1001–1014.
[7] [Online]. Available: https://www.ibm.com/quantum-computing/
[8] [Online]. Available: https://www.qiskit.org/
[9] A. Paler, "On the influence of initial qubit placement during NISQ circuit compilation," 2018, abs/1811.08985.
[10] X. Zhou, S. Li, and Y. Feng, "Quantum circuit transformation based on simulated annealing and heuristic search," *IEEE Transactions on Computer-Aided Design of Integrated Circuits and Systems*, vol. 39, no. 12, pp. 4683–4694, 2020.
[11] A. Kissinger and A. M. de Griend, "CNOT circuit extraction for topologically-constrained quantum memories," *Quantum Inf. Comput.*, vol. 20, no. 7&8, pp. 581–596, 2020.
[12] B. Nash, V. Gheorghiu, and M. Mosca, "Quantum circuit optimizations for NISQ architectures," *Quantum Science and Technology*, vol. 5, no. 2, p. 025010, 2020.
[13] D. Venturelli, M. Do, E. G. Rieffel, and J. Frank, "Temporal planning for compilation of quantum approximate optimization circuits," in *Proceedings of the 26th International Joint Conference on Artificial Intelligence*, 2017, pp. 4440–4446.

[14] D. E. Bernal, K. E. C. Booth, R. Dridi, H. Alghassi, S. R. Tayur, and D. Venturelli, "Integer programming techniques for minor-embedding in quantum annealers," in *Proceedings of the 17th International Conference on Integration of Constraint Programming, Artificial Intelligence, and Operations Research*, ser. Lecture Notes in Computer Science, vol. 12296. Springer, 2020, pp. 112–129.

[15] A. A. A. de Almeida, G. W. Dueck, and A. C. R. da Silva, "Finding optimal qubit permutations for IBM's quantum computer architectures," in *Proceedings of the 32nd Symposium on Integrated Circuits and Systems Design*. ACM, 2019, p. 13.

[16] P. Murali, N. M. Linke, M. Martonosi, A. Javadi-Abhari, N. H. Nguyen, and C. H. Alderete, "Full-stack, real-system quantum computer studies: architectural comparisons and design insights," in *Proceedings of the 46th International Symposium on Computer Architecture*. ACM, 2019, pp. 527–540.

[17] M. Y. Siraichi, V. F. dos Santos, S. Collange, and F. M. Q. Pereira, "Qubit allocation," in *Proceedings of the 2018 International Symposium on Code Generation and Optimization*. ACM, 2018, pp. 113–125.

[18] A. Shafaei, M. Saeedi, and M. Pedram, "Optimization of quantum circuits for interaction distance in linear nearest neighbor architectures," in *Proceedings of the 50th Annual Design Automation Conference*. ACM, 2013, pp. 41:1–41:6.

[19] G. G. Guerreschi and J. Park, "Two-step approach to scheduling quantum circuits," *Quantum Science and Technology*, vol. 3, no. 4, p. 045003, 03 2018.

[20] A. Matsuo and S. Yamashita, "An efficient method for quantum circuit placement problem on a 2-d grid," in *Proceedings of the 11th International Conference on Reversible Computation*, ser. Lecture Notes in Computer Science, vol. 11497. Springer, 2019, pp. 162–168.

[21] A. Cowtan, S. Dilkes, R. Duncan, A. Krajenbrink, W. Simmons, and S. Sivarajah, "On the qubit routing problem," in *Proceedings of the 14th Conference on the Theory of Quantum Computation, Communication and Cryptography*, ser. LIPIcs, vol. 135, 2019, pp. 5:1–5:32.

[22] S. S. Tannu and M. K. Qureshi, "Not all qubits are created equal: A case for variability-aware policies for nisq-era quantum computers," in *Proceedings of the 24th International Conference on Architectural Support for Programming Languages and Operating Systems*. ACM, 2019, pp. 987–999.

[23] O. Daei, K. Navi, and M. Z. Moghadam, "Optimized quantum circuit partitioning," *CoRR*, vol. abs/2005.11614, 2020.

[24] A. Barenco, C. Bennett, R. Cleve, D. DiVincenzo, N. Margolus, P. Shor, T. Sleator, J. Smolin, and H. Weinfurter, "Elementary gates for quantum computation," *Physical Review A*, vol. 52, no. 5, pp. 3457–3467, 1995.

[25] M. Möttönen and J. Vartiainen, *Decompositions of general quantum gates*. Nova Science Publishers Inc, 2006.

[26] Y. Zhang, H. Deng, Q. Li, H. Song, and L. Nie, "Optimizing quantum programs against decoherence: Delaying qubits into quantum superposition," in *2019 International Symposium on Theoretical Aspects of Software Engineering*. IEEE, 2019, pp. 184–191.

APPENDIX A
EXPERIMENTAL DETAILS OF THE ADDED SWAP GATE AND DEPTH OF THE OUTPUT CIRCUIT

The qubit no. indicates the number of qubits in the circuit, the CNOT no. indicates the number of initial CNOT gates, TSA_{num}, TSA_{dep}, optm, wghtgr, SABRE indicate the number of CNOT gates added by the TSA using their respective circuit transformation methods. Since wghtgr and SABRE do not count the depth of the converted circuit, no comparison is made. "-" means that the circuit cannot be successfully transformed within five minutes.

Table III and Table IV show the circuits that TSA_{num}, TSA_{dep}, optm, wghtgr can successfully transform, and calculate the total number of gates added by them. Table V shows the circuits that optm, wghtgr, and SABRE may not be able to handle. Table VI VII shows the depth of the circuit after TSA_{num}, TSA_{dep}, optm can be successfully transform. Table VIII shows the circuits that optm cannot handle.

Circuit name	qubit no.	CNOT no.	TSA$_{num}$ added	TSA$_{dep}$ added	optm added	wghtgr added	SABRE added
decod24-enable_126	6	149	28	42	60	16	129
4mod5-v0_19	5	16	0	0	0	0	-
4mod5-v0_18	5	31	2	5	4	4	-
mod5d2_64	5	25	5	6	8	3	-
4gt4-v0_72	6	113	14	10	33	14	-
alu-v3_35	5	18	2	4	8	2	-
4gt4-v0_73	6	179	27	34	76	12	-
alu-v3_34	5	24	2	3	7	2	-
3_17_13	3	17	0	0	6	0	0
4gt4-v0_78	6	109	12	8	48	4	124
4gt4-v0_79	6	105	17	17	48	3	-
4mod7-v1_96	5	72	16	19	27	7	-
mod10_171	5	108	17	20	39	9	-
ex2_227	7	275	48	59	121	33	-
mod10_176	5	78	14	14	38	8	-
0410184_169	5	9	2	2	49	3	-
4mod5-v0_20	5	10	0	0	4	0	-
aj-e11_165	5	69	8	8	33	7	63
alu-v1_28	5	18	2	4	11	2	-
4gt12-v0_86	6	116	28	33	48	3	-
4gt12-v0_87	6	112	27	32	45	2	-
4gt12-v0_88	6	86	5	5	25	4	-
alu-v1_29	5	17	4	4	11	2	13
ham7_104	7	149	28	34	68	12	-
C17_204	7	205	26	53	99	22	-
xor5_254	6	5	0	0	1	0	3
hwb4_49	5	107	14	15	38	11	157
rd73_140	10	104	23	26	35	20	-
decod24-v0_38	4	23	0	0	6	0	-
rd53_131	7	200	39	39	98	24	-
rd53_133	7	256	37	47	102	27	160
rd53_135	7	134	28	29	38	23	-
decod24-v2_43	4	22	0	0	9	0	39
rd53_138	8	60	14	16	23	9	-
rd32-v0_66	4	16	0	0	6	0	-
4gt13-v1_93	5	30	0	0	13	0	-
graycode6_47	6	5	0	0	0	0	-
4mod5-bdd_287	7	31	3	6	8	6	34
ham3_102	3	11	0	0	3	0	12
4gt4-v0_80	6	79	5	5	22	5	-
ex-1_166	3	9	0	0	3	0	-
mod5mils_65	5	16	0	0	6	0	-
0example	5	9	1	2	3	3	-
alu-v4_36	5	51	12	8	22	4	41
alu-v4_37	5	18	2	4	8	2	-
ex1_226	6	5	0	0	1	0	15
one-two-three-v0_98	5	65	11	13	32	10	-
one-two-three-v0_97	5	128	23	23	64	16	-
one-two-three-v3_101	5	32	3	4	14	3	-
rd32_270	5	36	3	3	6	6	24
rd53_130	7	448	89	100	190	49	-
rd53_251	8	564	104	131	230	45	-
4mod5-v1_24	5	16	0	0	3	0	-
mod5adder_127	6	239	21	56	111	20	-
4_49_16	5	99	20	17	40	10	-
hwb5_53	6	598	141	168	173	59	-
ex3_229	6	175	10	9	50	11	-
4gt10-v1_81	5	66	14	15	28	6	-
alu-v2_32	5	72	15	17	27	7	-
alu-v2_31	5	198	42	54	85	13	-
alu-v2_30	6	223	41	45	96	20	-
sf_276	6	336	12	52	138	12	-
decod24-v1_41	5	38	4	4	14	3	28
sf_274	6	336	34	21	82	12	-
4gt4-v1_74	6	119	17	24	37	9	-
alu-v2_33	5	17	4	4	8	2	-
cnt3-5_179	16	85	6	6	35	4	-

TABLE III: Comparison of the numbers of SWAP gates added by the output circuits on the IBM Q20

Circuit name	qubit no.	CNOT no.	TSA$_{num}$ added	TSA$_{dep}$ added	optm added	wghtgr added	SABRE added
decod24-v1_41	5	38	4	4	14	3	28
sf_274	6	336	34	21	82	12	-
4gt4-v1_74	6	119	17	24	37	9	-
alu-v2_33	5	17	4	4	8	2	-
cnt3-5_179	16	85	6	6	35	4	-
4mod5-v1_22	5	11	0	0	5	0	0
4mod5-v1_23	5	32	5	5	4	3	55
mini_alu_305	10	77	10	20	28	8	123
alu-v0_26	5	38	7	10	13	3	-
alu-bdd_288	7	38	4	12	16	6	-
alu-v0_27	5	17	2	4	11	2	9
4gt13_91	5	49	7	7	10	2	-
4gt5_77	5	58	12	12	20	6	-
4gt13_92	5	30	0	0	14	0	-
4gt5_76	5	46	7	10	24	5	39
4gt5_75	5	38	5	12	16	4	53
4gt12-v1_89	6	100	11	21	38	4	-
4gt11_83	5	14	0	0	0	0	-
mod5d1_63	5	13	0	0	1	0	-
4gt11_82	5	18	1	1	1	1	-
decod24-v3_45	5	64	15	15	32	8	64
rd32-v1_68	4	16	0	0	6	0	24
mini-alu_167	5	126	27	27	49	11	-
one-two-three-v2_100	5	32	3	4	8	3	-
4mod7-v0_94	5	72	8	13	36	9	-
cm82a_208	8	283	41	69	84	33	-
mod8-10_178	6	152	5	20	13	7	-
mod8-10_177	6	196	14	33	58	13	230
majority_239	7	267	39	43	105	33	-
miller_11	3	23	0	0	9	0	36
decod24-bdd_294	6	32	4	4	9	4	36
total	551	9244	1372	1738	3481	800	-

TABLE IV: Comparison of the numbers of SWAP gates added by the output circuits on the IBM Q20

Circuit name	qubit no.	CNOT no.	TSA_{num} added	TSA_{dep} added	optm added	wghtgr added	SABRE added
max46_240	10	11844	3473	4545	-	-	-
rd73_252	10	2319	586	761	-	-	-
cycle10_2_110	12	2648	919	1216	961	-	-
sqrt8_260	12	1314	379	492	457	-	-
urf4_187	11	224028	54785	60140	-	-	-
sqn_258	10	4459	1199	1420	-	-	-
f2_232	8	525	87	124	218	-	-
radd_250	13	1405	386	489	511	-	-
ham15_107	15	3858	1326	1689	-	-	-
sao2_257	14	16864	5346	7178	-	-	-
sym9_148	10	9408	1865	2432	-	-	-
urf5_280	9	23764	6989	8730	-	-	-
square_root_7	15	3089	812	2150	-	-	-
sys6-v0_111	10	98	23	26	38	-	-
hwb7_59	8	10681	2687	3551	3722	-	-
sym9_146	12	148	38	55	54	-	248
wim_266	11	427	93	120	147	-	-
urf2_152	8	35210	9181	11921	10577	-	-
urf5_159	9	71932	20258	25505	-	-	-
urf2_277	8	10066	2807	3798	3782	-	-
life_238	11	9800	2762	3576	-	-	-
root_255	13	7493	2128	3035	-	-	-
9symml_195	11	15232	4553	5986	-	-	-
sym10_262	12	28084	8534	11033	-	-	-
dc1_220	11	833	226	207	371	-	-
cm42a_207	14	771	182	229	294	-	-
rd53_311	13	124	26	48	47	-	-
dc2_222	15	4131	1383	1773	-	-	-
rd84_142	15	154	49	58	50	-	-
sym6_145	7	1701	317	449	750	-	-
co14_215	15	7840	3078	3819	-	-	-
cnt3-5_180	16	215	59	74	79	-	-
cm152a_212	12	532	103	129	168	-	-
sym6_316	14	123	30	39	56	-	-
mlp4_245	16	8232	2780	3490	-	-	-
hwb8_113	9	30372	10749	16489	-	-	-
qft_16	16	240	90	147	-	-	-
plus63mod4096_163	13	56329	19759	24273	-	-	-
urf1_149	9	80878	22551	28516	-	-	-
urf3_155	10	185276	50842	62903	-	-	-
urf3_279	10	60380	17999	23318	-	-	-
hwb9_119	10	90955	22946	30031	-	-	-
plus63mod8192_164	14	81865	28022	36207	-	-	-
pm1_249	14	771	182	229	294	-	-
sym9_193	11	15232	4382	5518	-	-	-
misex1_241	15	2100	480	754	600	-	-
urf1_278	9	26692	8010	10217	-	-	-
squar5_261	13	869	219	313	290	-	-
ground_state_estimation_10	13	154209	11671	22886	-	-	-
adr4_197	13	1498	516	670	-	-	-
hwb6_56	7	2952	698	933	909	-	-
clip_206	14	14772	5430	6865	-	-	-
cm85a_209	14	4986	2088	2225	-	-	-
rd84_253	12	5960	1849	2333	-	-	-
dist_223	13	16624	5623	7431	-	-	-
inc_237	16	4636	1193	1667	-	-	-
qft_10	10	90	23	34	30	-	-
urf6_160	15	75180	27524	32452	-	-	-
con1_216	9	415	86	118	177	-	-

TABLE V: Comparison of the numbers of SWAP gates added by the output circuits on the IBM Q20

Circuit name	qubit no.	CNOT no.	depths no.	TSA$_{num}$ depths	TSA$_{dep}$ depths	optm depths
decod24-enable_126	6	149	190	233	275	470
4mod5-v0_19	5	16	21	16	16	21
4mod5-v0_18	5	31	40	37	46	54
mod5d2_64	5	25	32	40	43	67
4gt4-v0_72	6	113	137	155	143	297
alu-v3_35	5	18	22	24	30	60
4gt4-v0_73	6	179	227	260	281	586
alu-v3_34	5	24	30	30	33	63
3_17_13	3	17	22	17	17	52
4gt4-v0_78	6	109	137	145	133	352
4gt4-v0_79	6	105	132	156	156	345
4mod7-v1_96	5	72	94	120	129	218
mod10_171	5	108	139	159	168	335
ex2_227	7	275	355	419	452	899
mod10_176	5	78	101	120	120	104
cycle10_2_110	12	2648	3386	5405	6296	7467
0410184_169	5	9	6	15	15	253
4mod5-v0_20	5	10	12	10	10	32
sqrt8_260	12	1314	1661	2451	2790	3561
aj-e11_165	5	69	86	93	93	250
alu-v1_28	5	18	22	24	30	70
f2_232	8	525	668	786	897	1672
radd_250	13	1405	1781	2563	2872	3985
4gt12-v0_86	6	116	135	200	215	334
4gt12-v0_87	6	112	131	193	208	324
4gt12-v0_88	6	86	108	101	101	222
alu-v1_29	5	17	22	29	29	64
ham7_104	7	149	185	233	251	491
C17_204	7	205	253	283	364	688
xor5_254	6	5	5	5	5	10
hwb4_49	5	107	134	149	152	308
rd73_140	10	104	92	173	182	185
decod24-v0_38	4	23	30	23	23	61
rd53_131	7	200	261	317	317	677
rd53_133	7	256	327	367	397	777
rd53_135	7	134	159	218	221	331
sys6-v0_111	10	98	75	167	176	188
decod24-v2_43	4	22	30	22	22	75
hwb7_59	8	10681	13437	18742	21334	29601
rd53_138	8	60	56	102	108	114
rd32-v0_66	4	16	20	16	16	51
rd53_135	7	134	159	218	221	331
sys6-v0_111	10	98	75	167	176	188
decod24-v2_43	4	22	30	22	22	75
hwb7_59	8	10681	13437	18742	21334	29601
rd53_138	8	60	56	102	108	114
rd32-v0_66	4	16	20	16	16	51
sym9_146	12	148	127	262	313	309
4gt13-v1_93	5	30	39	30	30	102
graycode6_47	6	5	5	5	5	5
wim_266	11	427	514	706	787	1180
urf2_152	8	35210	44100	62753	70973	90299
urf2_277	8	10066	11390	18487	21460	26548
4mod5-bdd_287	7	31	41	40	49	71
ham3_102	3	11	13	11	11	28
4gt4-v0_80	6	79	101	94	94	206
ex-1_166	3	9	12	9	9	28
mod5mils_65	5	16	21	16	16	52
0example	5	9	6	12	15	15
alu-v4_36	5	51	66	87	75	170
alu-v4_37	5	18	22	24	30	60
ex1_226	6	5	5	5	5	10
one-two-three-v0_98	5	65	82	98	104	234
one-two-three-v0_97	5	128	163	197	197	443
one-two-three-v3_101	5	32	40	41	44	95
rd32_270	5	36	47	45	45	76

TABLE VI: Comparison of the depths of the output circuits on the IBM Q20

Circuit name	qubit no.	CNOT no.	depths no.	TSA$_{num}$ depths	TSA$_{dep}$ depths	optm depths
dc1_220	11	833	1041	1511	1454	2711
rd53_130	7	448	569	715	748	1417
rd53_251	8	564	712	876	957	1767
cm42a_207	14	771	940	1317	1458	2279
rd53_311	13	124	130	202	268	300
4mod5-v1_24	5	16	21	16	16	36
mod5adder_127	6	239	302	302	407	817
4_49_16	5	99	125	159	150	320
hwb5_53	6	598	758	1021	1102	1560
ex3_229	6	175	226	205	202	462
rd84_142	15	154	110	301	328	253
4gt10-v1_81	5	66	84	108	111	210
alu-v2_32	5	72	92	117	123	215
alu-v2_31	5	198	255	324	360	650
alu-v2_30	6	223	285	346	358	734
sym6_145	7	1701	2187	2652	3048	5716
sf_276	6	336	435	372	492	1096
decod24-v1_41	5	38	50	50	50	120
sf_274	6	336	436	438	399	822
4gt4-v1_74	6	119	154	170	191	329
alu-v2_33	5	17	22	29	29	59
cnt3-5_180	16	215	209	392	437	482
cm152a_212	12	532	684	841	919	1423
cnt3-5_179	16	85	61	103	103	166
sym6_316	14	123	135	213	240	378
4mod5-v1_22	5	11	12	11	11	37
4mod5-v1_23	5	32	41	47	47	55
mini_alu_305	10	77	71	107	137	187
alu-v0_26	5	38	49	59	68	108
alu-bdd_288	7	38	48	50	74	112
alu-v0_27	5	17	21	23	29	63
4gt13_91	5	49	61	70	70	108
4gt5_77	5	58	74	94	94	170
4gt13_92	5	30	38	30	30	103
4gt5_76	5	46	56	67	76	171
4gt5_75	5	38	47	53	74	127
4gt12-v1_89	6	100	130	133	163	313
one-two-three-v1_99	5	59	76	95	89	194
4gt13_90	5	53	65	74	74	124
pm1_249	14	771	940	1317	1458	2279
ising_model_10	10	90	52	90	90	107
misex1_241	15	2100	2676	3540	4362	5326
4gt11_84	5	9	11	9	9	25
4gt11_83	5	14	16	14	14	16
mod5d1_63	5	13	13	13	13	17
4gt11_82	5	18	20	21	21	25
squar5_261	13	869	1051	1526	1808	2309
decod24-v3_45	5	64	84	109	109	244
rd32-v1_68	4	16	21	16	16	52
hwb6_56	7	2952	3736	5046	5751	7773
mini-alu_167	5	126	162	207	207	400
one-two-three-v2_100	5	32	40	41	44	80
4mod7-v0_94	5	72	92	96	111	270
cm82a_208	8	283	340	406	490	699
mod8-10_178	6	152	193	167	212	243
mod8-10_177	6	196	251	238	295	525
majority_239	7	267	344	384	396	839
qft_10	10	90	37	159	192	135
miller_11	3	23	29	23	23	75
decod24-bdd_294	6	32	40	44	44	86
con1_216	9	415	508	673	769	1197
total	823	83416	103023	145372	164848	224731

TABLE VII: Comparison of the depths of the output circuits on the IBM Q20

Circuit name	qubit no.	CNOT no.	depths no.	TSA$_{num}$ depths	TSA$_{dep}$ depths	optm depths
max46_240	10	11844	14257	22263	25479	-
rd73_252	10	2319	2867	4077	4602	-
urf4_187	11	224028	264330	388383	404448	-
sqn_258	10	4459	5458	8056	8719	-
ham15_107	15	3858	4819	7836	8925	-
sao2_257	14	16864	19563	32902	38398	-
sym9_148	10	9408	12087	15003	16704	-
urf5_280	9	23764	27822	44731	49954	-
square_root_7	15	3089	3847	5525	9539	-
urf5_159	9	71932	89148	132706	148447	-
life_238	11	9800	12511	18086	20528	-
root_255	13	7493	8839	13877	16598	-
9symml_195	11	15232	19235	28891	33190	-
sym10_262	12	28084	35572	53686	61183	-
dc2_222	15	4131	5242	8280	9450	-
co14_215	15	7840	8570	17074	19297	-
mlp4_245	16	8232	10328	16572	18702	-
hwb8_113	9	30372	38717	62619	79839	-
qft_16	16	240	61	510	681	-
plus63mod4096_163	13	56329	72246	115606	129148	-
urf1_149	9	80878	99586	148531	166426	-
urf3_155	10	185276	229365	337802	373985	-
urf3_279	10	60380	70702	114377	130334	-
hwb9_119	10	90955	116199	159793	181048	-
plus63mod8192_164	14	81865	105142	165931	190486	-
sym9_193	11	15232	19235	28378	31786	-
ising_model_13	13	120	46	120	120	-
urf1_278	9	26692	30955	50722	57343	-
ising_model_16	16	150	57	150	150	-
ground_state_estimation_10	13	154209	217236	189222	222867	-
adr4_197	13	1498	1839	3046	3508	-
clip_206	14	14772	17879	31062	35367	-
cm85a_209	14	4986	6374	11250	11661	-
rd84_253	12	5960	7261	11507	12959	-
dist_223	13	16624	19694	33493	38917	-
inc_237	16	4636	5864	8215	9637	-
urf6_160	15	75180	93645	157752	172536	-

TABLE VIII: Comparison of the depths of the output circuits on the IBM Q20